Systematic Study of Solid-State U(VI) Photoreactivity: Long-Lived Radicalization and Electron Transfer in Uranyl Tetrachloride

Jordan A. Herder, Samantha J. Kruse, Aaron D. Nicholas, Tori Z. Forbes, Eric D. Walter, Herman Cho, and Christopher L. Cahill*

ABSTRACT: Reported are the syntheses, structural characterizations, and luminescence properties of three novel $[UO_2Cl_4]^{2-}$ bearing compounds containing substituted 1,1′-dialkyl-4,4′-bipyridinum dications (i.e., viologens). These compounds undergo photoinduced luminescence quenching upon exposure to UV radiation. This reactivity is concurrent with two phenomena: radicalization of the uranyl tetrachloride anion and photoelectron transfer to the viologen which constitutes the formal transfer of one electron from $[UO_2Cl_4]^{2-}$ to the viologen species. This behavior is elucidated using electron paramagnetic resonance (EPR) spectroscopy and further probed through a series of characterization and computational techniques including Rehm−Weller analysis, time-dependent density functional theory (TD-DFT), and density of states (DOS). This work provides a systematic study of the photoreactivity of the uranyl unit in the solid state, an under-described aspect of fundamental uranyl chemistry.

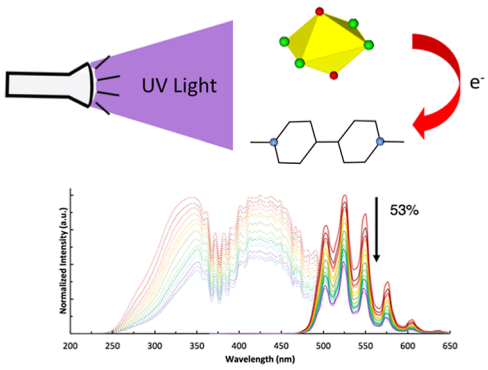

INTRODUCTION

The photophysical properties of uranium, specifically those of the uranyl cation (UO_2^{2+}), have been a fruitful area of study for actinide chemists for decades. Luminescence in particular provides a useful tool with which to probe the electronic structure of uranyl-bearing materials and has been helpful in delineating the structure−property relationships in a variety of settings. These properties arise from the presence of 5f orbitals and their ability to participate in bonding with the terminal oxygens and to a lesser extent their equatorial ligands. UO_2^{2+} can also facilitate photoreactivity in both solution and the solid state. Researchers have leveraged these aspects of actinide chemistry to elicit interesting properties in a range of systems and rationalize the behavior observed in, for example, catalysis, speciation, and radiation detection.[1−5] Our previous work has capitalized on the ability of UO_2^{2+} to prompt in situ peroxide formation in order to make novel families of solid-state complexes.[3] Indeed, this is a well-understood phenomenon whereby UO_2^{2+} is excited by incident light to make a strongly oxidizing species that participates in hydrogen abstraction (with a suitable substrate) and subsequently reduces ambient oxygen,[6] ultimately resulting in radicalized substrate species and peroxide ions.

Still more work has been committed to immobilizing UO_2^{2+} with ancillary ligands in order to channel its photoreactive properties in solid-state materials and metal organic frameworks, which allows uranium to execute diverse functions.[4,7−10] Researchers have utilized such systems for applications including the degradation of organic dyes, catalysis of organic reactions, and use in radiation detection devices.[7] What has become clear from these efforts is that UO_2^{2+} photoreactivity extends to both the solution state and the solid state, yet the mechanisms by which these processes occur are varied. Some heterocatalytic materials allow UO_2^{2+} to carry out the role described by Espenson et al. (and described above).[6] Other materials favor a prolonged radicalization of ligands which manifests itself as luminescence quenching,[9] whereas others evoke long-lived reduced uranium metal centers.[8] The mechanism proposed by Espenson et al. likely describes the majority of the activity seen in uranyl-bearing systems in the solution state, yet a similarly encompassing description for photoreactive solid-state materials remains elusive. Thus, there is a need to synthesize new photoreactive uranyl materials and probe the relevant properties and mechanisms therein.

The uranyl tetrachloride ($[UO_2Cl_4]^{2-}$) anion is a prime candidate with which to probe the photoreactivity of solid-state uranyl-bearing materials. This unit has well-understood optical and chemical properties and has been studied extensively for its propensity to form supramolecular networks with organic cations such as pyridinium derivatives.[12−14]

Building on these efforts, we herein introduce viologens to form analogous materials, which may capitalize on their well-established electronic properties, as utilized in catenanes, molecular switches and machines, and photochromic materials.[15−17] Viologens act as one- or two-electron acceptors by providing energetically accessible π^* orbitals that are reduced via photoelectron transfer (PET). PET is the process whereby an excited electron, from an electron-rich donor species, is transferred to and subsequently reduces the acceptor species, forming a stable redox product. Owing to conjugation about the aromatic rings, the reduced viologen radicals are particularly stable in these reactions.

There is extensive literature precedent for the photoreactivity evoked by utilizing the viologen unit in hybrid materials.[18−20] Examples include photochromic zinc materials[17] and more recently redox-active lanthanide materials.[21] Turning to the actinides, and the uranyl unit in particular, examples are more scarce.[22−24] These examples utilize the viologen and UO_2^{2+} for both their photochemical and structural contributions, yet lack an investigation of the underlying interactions between the two motifs. As such, we see an opportunity to synthesize uranyl-viologen-bearing materials with a focus on the fundamental photoreactivity as influenced by these two units.

The synthesis and characterization of three novel uranyl compounds that feature $[UO_2Cl_4]^{2-}$ units paired with methyl (MV), ethyl (EV), and propyl (PV) viologen dications are reported herein. These compounds exhibit typical green uranyl emission behavior which can be quenched via prolonged irradiation with UV light. Kinetic studies demonstrate that this process occurs via a second-order reaction whose rate constant is dependent on the viologen substituent. We postulate that exposure to UV light gives rise to a PET process whereby the $[UO_2Cl_4]^{2-}$ unit is oxidized to an air-stable radical $[UO_2Cl_4]^{-}$ species via electron transfer to the viologen. A PET mechanism is proposed and explored through a hybrid experimental and computational approach. EPR provides direct experimental evidence for the generation of organic centered radicals as a result of prolonged UV irradiation. Moreover, our results demonstrate that the photoinduced redox reaction between $[UO_2Cl_4]^{2-}$ and viologen ion pairs is (i) thermodynamically favorable and (ii) possible owing to the band structure and excited-state transitions. To our knowledge, this is the first report of a long-lived radical $[UO_2Cl_4]^{-}$ species.

EXPERIMENTAL SECTION

General. *Safety Statement. Caution!* $Cs_2UO_2Cl_4$ and $UO_2(CH_3CO_2)_2$: these compounds contain depleted U, and as such, standard precautions and protective measures should be taken when handing this radioactive and toxic heavy metal.

Synthesis. *Cesium Uranyl Tetrachloride.* Uranyl acetate ($C_4H_6O_6U$) (0.6240 g, 1.471 mmol) and CsCl (0.4959 g, 2.945 mmol) were dissolved in 10 mL of a 6 M HCl solution and heated to dryness to form long yellow shard-like crystals. The product was collected and characterized by PXRD to verify the product purity (compared to ICSD #56859; Figure S1) and used for subsequent syntheses.

Methyl Viologen Dichloride Hydrate. The reagent was purchased from Sigma-Aldrich (99% purity).

Ethyl- and Propyl-Viologen Diiodide. The corresponding alkyl iodides, ethyl iodide (C_2H_5I) (0.35 mL, 0.68 g, 4.4 mmol) in the synthesis of EV and propyl iodide (C_3H_7I) (0.42 mL, 0.75 g, 4.4 mmol) in the synthesis of PV, were combined with 4,4′-bipyridine ($C_{10}H_8N_2$) (EV: 0.3345 g, 2.142 mmol; PV: 0.3332 g, 2.133 mmol) in a 100 mL round-bottom flask. The reactants were dissolved in 20 mL of acetonitrile, stirred, and heated to reflux for 24 h. The solution was cooled, and the solid product, an orange powder (EV) or a dark red powder (PV), was filtered and washed with ethyl acetate.[25] Purity was confirmed by powder X-ray diffraction (PXRD) as compared to the simulated patterns from single-crystal diffraction analysis (Figures S2 and S3).

Compounds ***1*****−****3****, [$C_{12}H_{14}N_2$][UO_2Cl_4]; [$C_{14}H_{18}N_2$][UO_2Cl_4]; and [$C_{16}H_{22}N_2$][UO_2Cl_4].* Preparations followed the general procedure of combining $Cs_2UO_2Cl_4$ and the corresponding viologen in a 1:1 molar ratio conducted on a 0.1 mmol or 0.2 mmol scale. A specific example of this synthesis is as follows: $Cs_2UO_2Cl_4$ (0.0668 g, 0.0986 mmol; 0.0677 g, 0.0999 mmol; and 0.0679 g, 0.100 mmol for **1**−**3**, respectively) was combined with the corresponding viologen-halide salts: (**1**) methyl viologen dichloride hydrate ($C_{12}H_{14}N_2Cl_2{\cdot}H_2O$) (0.102 mmol, 0.0263 g); (**2**) ethyl viologen diiodide ($C_{14}H_{18}N_2I_2$) (0.103 mmol, 0.0482 g); and (**3**) propyl viologen diiodide ($C_{16}H_{22}N_2I_2$) (0.102 mmol, 0.0505 g) and dissolved in 3 mL of water. Slow evaporation of the solution from a Petri dish yielded yellow block crystals (**1** and **2**) and dark-yellow shard-like crystals (**3**) after 10 days. The PXRD patterns of bulk samples were compared to the calculated patterns, based on the SCXRD data of **1**−**3**, to verify the product purity (Figures S4−S6). Crystals were physically separated and harvested for further analysis.

X-ray Crystallography. Crystals of sufficient quality were collected from each corresponding reaction and mounted on MiTeGen micromounts. X-ray diffraction data were collected at 100 K on a Bruker D8 Quest equipped with an Incoatec IμS 3.0 Microfocus X-ray source (Mo Kα, λ = 0.71073 Å) and a Photon II detector. ShelXT was used to determine the molecular structure via intrinsic phasing methods through the APEX III software package.[26] Further structural refinements were carried out using SHELXL-2014 in the program ShelXle.[27] Hydrogen atoms were placed in idealized positions for aromatic, secondary, and primary carbons, respectively, and allowed to ride on their parent atoms. Relevant structural and refinement data, including unit cell parameters and collection conditions, are listed in Table 1 and crystallographic information files (CIFs) have been deposited with the Cambridge Structural Database. Moreover, we include (as Supporting Information) four additional CIFs of compounds **1** and **2** pre- and postirradiation to highlight the absence of significant structural changes upon UV light exposure. We note that **3** exhibited significant positional disorder of both the uranyl tetrachloride anion and the viologen molecule. The interatomic distances have been expressed as ranges of possible

Table 1. Crystal Structure and Refinement Data for 1−3

	1	2	3
CCDC ref code	2118265	2118266	2118267
formula	$[C_{12}H_{14}N_2][UO_2Cl_4]$	$[C_{14}H_{18}N_2][UO_2Cl_4]$	$[C_{16}H_{22}N_2][UO_2Cl_4]$
formula weight (g)	598.08	626.13	654.18
crystal system	monoclinic	triclinic	orthorhombic
space group	$P2_1/n$	$P\bar{1}$	$Pnnm$
a (Å)	6.8889(3)	8.1393(8)	8.7757(4)
b (Å)	10.9983(5)	8.1541(8)	13.8926(6)
c (Å)	11.1155(4)	8.6929(8)	8.5361(4)
α (°)	90	108.605(3)	90
β (°)	90.3850(10)	117.112(3)	90
γ (°)	90	93.241(3)	90
volume (Å^3)	842.16(6)	472.55(8)	1040.70(8)
Z	2	1	2
radiation	Mo Kα (0.71073 Å)	Mo Kα (0.71073 Å)	Mo Kα (0.71073 Å)
temperature (K)	100(2)	100(2)	100(2)
R_1	0.0143	0.0118	0.0493
R_{int}	0.0283	0.0306	0.0405

interaction lengths, and errors associated with distances are omitted. Details of the disorder are included in the CIF of **3**.

Powder X-ray Diffraction. PXRD data were collected on ground bulk samples using a Rigaku MiniFlex 6G Benchtop X-ray diffraction system in the SmartLab Studio II software suite. Patterns were collected with Cu Kα (λ = 1.5406 Å) radiation from samples mounted on zero-background silicon sample holders. The data were subsequently processed with the Match! 3 software package.[28]

Optical Measurements. Diffuse reflectance spectra were collected using Mikropack DH-2000-BAL deuterium and halogen lamps generating light that was delivered and collected with a fiber−optic cable. An Ocean Optics flame detector was used to analyze the scattered light. Spectra were collected on samples **1**−**3** at 298 K while resting on a $BaSO_4$ pressed pellet, which served as a reference material. Data were processed using OceanView spectroscopy software, and Tauc plots of reflection data were generated. Steady-state luminescence scans of **1**−**3** were collected at 298 K with a Fluorolog-3 photoluminescence spectrophotometer from Horiba using a 450 W xenon arc lamp combined with a double-excitation monochromator and a double-emission monochromator. A photomultiplier tube at 950 V was used as the emission detector.

Kinetic Measurements. Kinetic data were obtained via monitoring the luminescence emission spectra over time as samples were irradiated with UV light. Irradiation was achieved using a 450 W xenon arc source and a double-excitation monochromator. Excitation monochromators were fixed at 345 nm for **1** and 325 nm for **2** and **3**, with 14 nm slit widths for the light apertures, to achieve sufficient irradiation. Emission spectra were measured at various time intervals using the maximum excitation values of 345 nm for **1** and 325 nm for **2** and **3**. Emission intensity values were taken from the emission maximum at 525 nm for **1** and 524 nm for **2** and **3**. Kinetic experiments on **1**−**3** were repeated three times with fresh material, and the average of the data was obtained. To compare the kinetic data to a nonviologen-bearing system, three control experiments were performed on $Cs_2UO_2Cl_4$, with the excitation and emission wavelengths of 350 and 522 nm, respectively.

Electron Paramagnetic Resonance. EPR spectra were collected using a Bruker EMX EPR spectrometer equipped with a Bruker HS EPR cavity operated with WinEPR software. Samples were purged with argon and sealed in quartz NMR tubes. The magnetic field was centered at 3500.00 G with a sweep width of 500.00 G, 60.0 s sweep time, and sample *g*-factor of 2.000. Frequency was maintained at approximately 9.84 MHz, microwave attenuation was set to 20 dB, and power was set to 2.00 mW. Modulation amplitude and frequency were set to 1.000 G and 100.00 kHz, respectively. Five accumulations were collected and averaged to generate individual spectra and converted to absorbance. OriginPro 9.60 (OriginLab, Northampton, MA) 64 bit software package was used to fit the peaks to Lorentzian functions and refine the fitting parameters to convergence. Irradiation was achieved by placing sealed samples into a resonator, with optical access via a slotted front cover, and directing light from an Ace Glass 450 W Mercury-arc lamp (with a flux of 50 mW/cm^2) onto the sample for specified periods of time (0, 5, 15, 20, 60, 120, and 180 min).

Raman Analysis. Raman spectra of single crystals of **1**−**3** were recorded using a HORIBA LabRAM HR Evolution Raman microscope over the range of 200−2000 cm^{-1}. An excitation line at 532 nm was used for each collection with a laser power of 1−5%. Irradiation was achieved using light from Dymax BlueWave 200 V 3.1 lamp.

Cyclic Voltammetry. Cyclic voltammetry was performed on viologen starting materials to obtain consistent data pertaining to their reduction potentials, specifically that of the first reduction from the dicationic species (RV^{2+}) to the monocationic species ($RV^{\bullet+}$). Analysis was conducted on 1 mM solutions of viologen reagent in 1 M KCl aqueous electrolyte solution with a glassy carbon working electrode (3 mm diameter), Ag/AgCl reference electrode in 4 M AgCl filling solution, and a platinum counter electrode. The solution was degassed using argon to purge the system of dissolved oxygen. Measurements were conducted using a BAS CV-50W voltammetric analyzer equipped with a C3 Cell Stand at 200 mV/s sweep speed through ranges appropriate for each viologen reagent measured. Voltammograms can be found in the Supporting Information of this article.

Computational Methods. Density functional theory (DFT) and time-dependent density functional theory (TD-DFT) were used to calculate optimized structures and molecular orbital transitions from the truncated models of **1**−**3** (Figure S7, Supporting Information) and free-energy values for ions in various oxidation states. Calculations were performed in the Gaussian 16 software (Gaussian Inc.)[29] using the B3LYP[30,31] functional with the def2-TZVP basis set for all Cl atoms,[32] the 6-311G(d,p) basis set for all C/H/N/O atoms,[33] and the scalar Stuttgart energy-consistent relativistic 32 valence electron pseudopotential and associated ECP60MWB_SEG valence basis set for U atoms.[34−36] Isodensity representations of molecular orbitals were rendered using the Avogadro (v1.2.0) software,[37] and the calculated ground-state parameters and full molecular orbital diagrams can be found in the Supporting Information. Density of state (DOS) calculations were performed on **1**−**3** using periodic boundary conditions in Gaussian 16 on crystallographically determined unit cells. DOS calculations were carried out via the HSE06[38−43] method utilizing the Heyd−Scuseria−Ernzerhof (HSE) hybrid combined with the Perdew, Burke, and Ernzerhof (PBE) exchange and correlation functions as well as the abovementioned basis sets. Total density of states (TDOS) and partial density of states (PDOS) data were extracted and analyzed using the Multiwfn program.[44] The TDOS was delineated into select PDOS components consisting of the U s/p, d, and f shells, the viologen π and π^* (p shell) molecular orbitals, and the halide p shell.

RESULTS AND DISCUSSION

Local Structure. The $[UO_2Cl_4]^{2-}$ anion is common to **1**−**3** and features a central square bipyramidal uranyl cation coordinated equatorially by four chloride ligands (Figure 1).

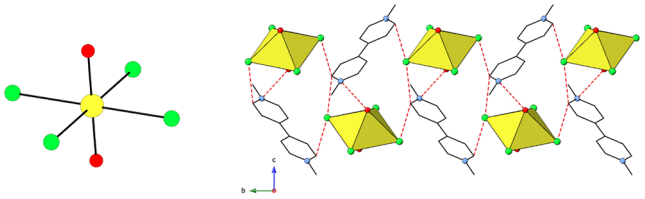

Figure 1. Left: Ball and stick representation of the tetrachloro uranyl dianion showing the U(VI) (yellow) center coordinated axially to two O (red) ligands and equatorially to four Cl (green) ligands. Right: Polyhedral representation of the assembly of compound **1**. Noncovalent interactions are highlighted by red dashed lines. Uranium metal centers are represented by yellow polyhedra. Color scheme: N, blue; O, red; Cl, green. Hydrogen atoms have been omitted for clarity.

The average U−O length is 1.76 Å, whereas the average U−Cl bond is 2.67 Å with no appreciable differences between uranyl anions in **1**−**3**, whose complete crystallographic parameters are listed in Tables S1−S3.

Crystal Structure Descriptions. Compound **1**, $(C_{12}H_{14}N_2)(UO_2Cl_4)$, crystallizes in the monoclinic space group, $P2_1/n$, where both the uranyl anion and viologen cation lie on the centers of inversion (Figure 1). This bimolecular salt is assembled in large part by simple anion−cation attractive forces, yet with a modicum of noncovalent interactions (NCIs), which may facilitate charge transfer (below). These include halogen···π and oxo···π interactions (lone-pair···π interactions), characterized by the overlap of the van der Waals (vdW) radii of an electron-rich atom (Cl/O) and an atom from an aromatic ring (C/N), and the lone pair donor species being positioned nearly perpendicular to the face of the ring.[45] Of these, there are one halogen···π and one oxo···π

interaction, with the ligand-to-ring distances of 3.382(3) Å (Cl1···C5), 3.007(3) Å (O1···N1), and 3.019(3) Å (O1···C1). These distances represent 98, 98, and 94% of the vdW radii sum, respectively. Figure 1 shows the packing and relevant NCIs between the $[UO_2Cl_4]^{2-}$ anions and neighboring MV^{2+} cations.

Compound **2** $(C_{14}H_{18}N_2)(UO_2Cl_4)$ crystallizes in the triclinic space group $P\bar{1}$. Like **1**, the interactions between molecules in **2** are largely electrostatic (Figure 2). While short

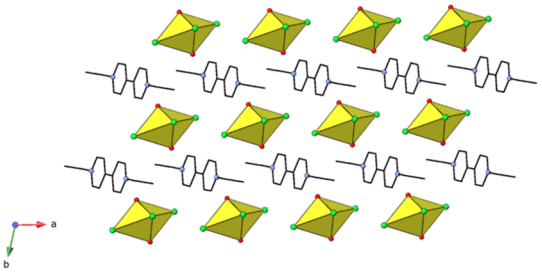

Figure 2. Polyhedral representation of the crystal structure of **2**, shown along the *c*-axis.

contacts between uranyl ligands and the aromatic viologen atoms are observed (Cl···C/N), no contact has the appropriate orientation, as described above, to be considered a halogen/oxo···π interaction. The molecular units assemble in the alternating sheets of $[UO_2Cl_4]^{2-}$ anions in the (010) planes and the viologen cations composing the (020) planes (Figure 2).

Compound **3** $(C_{16}H_{22}N_2)(UO_2Cl_4)$ crystallizes in the orthorhombic space group *Pnnm*. Figure 3 shows the assembly

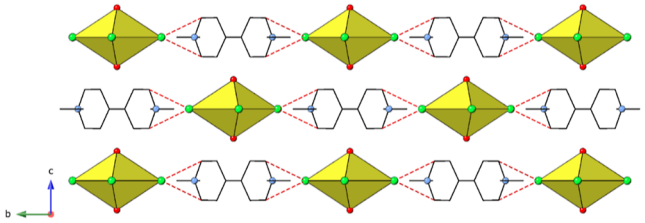

Figure 3. Polyhedral representation of the crystal packing in compound **3**, shown along the *a*-axis. Halogen···π interactions are highlighted by red dashed lines. Some disorder is present in the propyl viologen units (not shown).

of this compound which features a single NCI of note, a halogen···π interaction between a chloride ligand and the π-system of a neighboring viologen. This interaction has a range of distances and angles [3.448−3.493 Å (Cl to π-centroid distance), 99.80−102.03° (∠C-*centroid*-Cl)], owing to positional disorder in the modeling, but at its nearest occurrence of 3.448 Å, qualifies as a halogen···π interaction, albeit quite weak.[45] $[UO_2Cl_4]^{2-}$ units are flanked, along the *b*-axis, by propyl viologen cations that accommodate the lone Cl···π NCI. This alternating anion−cation motif creates nearly discrete 2D sheets along the (001) plane.

Optical Properties. Solid-state diffuse reflectance spectra were collected at room temperature on compounds **1**−**3** (Figure 4). The reflectance profiles, in all cases, feature a strong, broad absorption band in the UV region which extends into the visible region. The optical absorption edge decreases with the cation size on the order of **1** > **2** > **3** at 2.44, 2.18, and 2.09 eV, respectively (Figure S8). The absorption edge value is surmised to be dependent on the viologen species, owing to the common uranyl species in each compound, and would comport with the typical viologen behavior where larger or weaker electron-donating substituents tend to lead to smaller band gap energies.[46] It is worth noting that the known uranyl tetrachloride absorption bands centered around 320 nm (3.87 eV) and 420 nm (2.95 eV) overlap with those of the viologen cations, demonstrating that the higher lying filled orbitals of the ion pairs are similar in energy.

The excitation and emission spectra (Figure 4) show typical uranyl luminescence features across **1**−**3**. The excitation profiles of the materials show two broad excitation peaks centered at 345 and 420 nm corresponding to the ligand-to-metal charge-transfer (LMCT) bands associated with the equatorial chlorides and axial oxygens, respectively. Specifically, these bands arise owing to the electronic transition from the ground-state uranyl bonding orbitals ($3\sigma_u$, $3\sigma_g$, $1\pi_g$, and $2\pi_u$) to nonbonding U(VI) 5f δ_u and ϕ_u orbitals.[47] The finger-like peaks observed in the emission profile, like those in the excitation spectra, result from vibronic coupling to the symmetric U−O stretch. Notably, compounds **2**, **3**, and, to a lesser extent, **1** display additional vibronic features in the emission band, which correspond to coupled U−Cl vibrational modes (a phenomenon we have reported previously for other uranyl tetrachloride-containing materials).[14,48,49] There are notable differences in the excitation profiles across **1**−**3** (Figure 4, right), namely, the excitation bands vary in relative intensities as the identity of the viologen changes. For example, in **1**, the axial and equatorial excitation bands are similar in intensity, whereas for **3**, the equatorial excitation band is much higher in intensity than the axial band. A reduction in the relative band intensity of the low-energy axial band is indicative of more efficient equatorial ligand charge transfer resulting in emission (as opposed to nonradiative decay). This phenomenon is more pronounced in the compounds with larger viologen substituents, though the reason for this trend is not clear.

Kinetics. At the beginning of this study of pairing the uranyl tetrachloride anion with various viologens, it was unclear how the latter would influence the optical properties of the uranyl species. During the course of luminescence characterization, however, it became clear that the high-energy excitation band (the most intense band in compounds **1**−**3**) began red-shifting as the spectrum acquisition time increased. This was observed in addition to a discernible *decrease* in the overall emission intensity. Probing these observations further indicated that the luminescence profiles of the materials were changing, the degree to which was influenced by the amount of time the sample was irradiated. These observations, which from our perspective were not anticipated features of uranyl tetrachloride-containing materials, prompted a deeper and more systematic experimental inquiry, as well as a computational effort to rationalize the observed behavior.

Exposure of **1**−**3** to UV light leads to the gradual quenching of uranyl emission intensity over time. This phenomenon was investigated by measuring the emission and excitation of **1**−**3** at 5−30 min intervals over the course of 3 h of UV irradiation (Figure 5), and it was observed that the overall intensity reduction occurs on the order of **1** < **2** < **3** at 53, 67, and 84%, respectively (**3** displaying the most diminished emission). The excitation spectra reflect the loss of intensity of the emission; however, we note a difference in the relative reduction of the

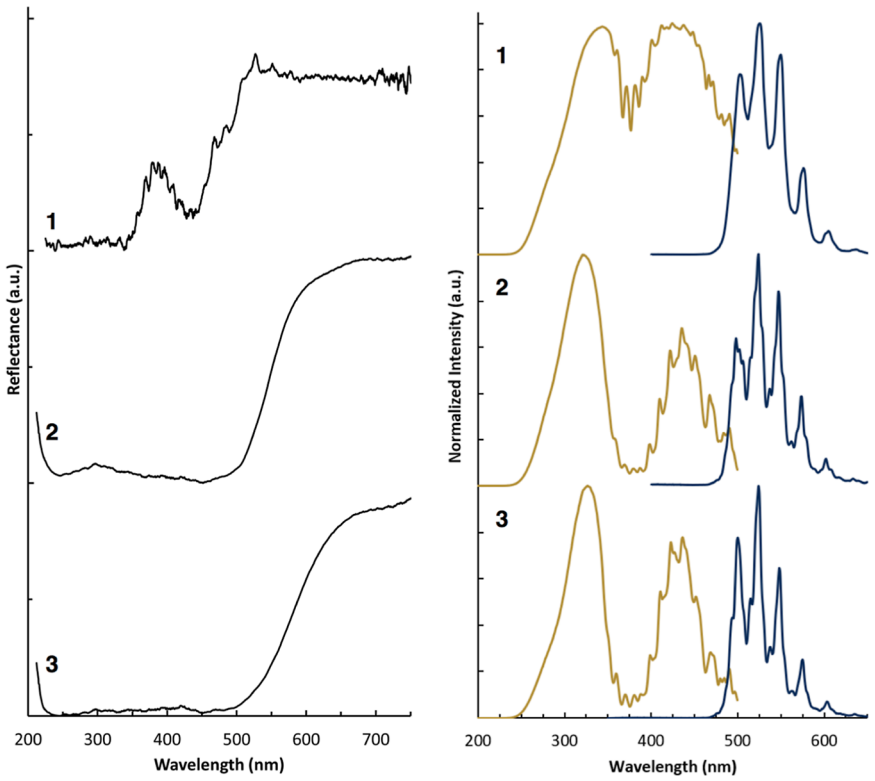

Figure 4. Diffuse reflectance (left) and photoluminescence (right) spectra of compounds **1**−**3** at 298 K. Excitation spectra are shown in gold, and emission spectra are shown in blue. The size of the viologen species (**3** > **2** > **1**) corresponds to a greater relative intensity of the high-energy excitation band (~335 nm), indicating that the charge transfer in the chloride ligand, relative to that of oxygen, occurs to a greater extent in the emissive species, as the viologen size increases. The excitation/emission wavelengths for **1**−**3** are 345 nm/526 nm, 325 nm/524 nm, and 325 nm/525 nm, respectively.

axial and equatorial bands. The equatorial charge-transfer excitation band (250−350 nm) undergoes red-shifting and is dramatically reduced relative to the axial charge-transfer excitation band (400−475 nm). This is most obvious in **3**, where the axial band intensity is reduced by ~33% and the equatorial is reduced by ~70%. Interestingly, the emission quenching was partially reversed by allowing the sample to remain in a dark environment overnight, and after 20 h, a notable portion of the luminescence intensity was recovered in all samples (7−21% recovery of max emission intensity; Figure S9, Supporting Information). A subsequent study shows that recovery is likely driven by exposure to atmospheric conditions (most likely oxygen) but is not investigated exhaustively in this report. Additional experiments investigating the effect of irradiation at the axial excitation band (~430 nm) are included in the Supporting Information.

The rate of emission quenching decreases significantly after 2 h of exposure, with no further quenching after 3 h. Time-dependent emission quenching of **1**−**3** obeys second-order reaction kinetics: $1/[(I_t - I_\infty)/(I_0 - I_\infty)] - 1/(I_0 - I_\infty) = kt$, where k is the second-order rate constant, and I_0, I_t, and I_∞ are the intensity values at time zero, time t, and the equilibrium point, respectively. This is consistent with the bimolecular process of electron transfer between molecular units, including viologen-containing materials.[50−52] We have plotted this relationship in Figure 6 and determined the rate constants of **1**−**3** to be 0.0458, 0.0461, and 0.076 mol^{-1} min^{-1}, respectively. It is worth noting that while rate laws are often helpful in explaining reactivity in the aqueous state, it is less helpful in describing the dynamics of our solid-state system beyond establishing a metric by which to rank reactivity.

It is clear that **3** experiences the most rapid quenching, while **1** and **2** are much slower with equivalent rates. Given the similarity of the uranyl anions in **1**−**3**, we attribute the difference in rates to the viologen species. It is worth noting that while this reactivity is the result of electron transfer to the viologen, the rate at which quenching occurs does not trend with the reduction potential of the corresponding viologen cation (reduction potential decreases from MV to PV to EV, with values of −582, −620, and −628 mV, respectively). This suggests that the properties of the viologen alone do not account for all changes to reactivity, and that rate may be influenced by factors such as structural assembly or other solid-state effects. As the luminescence arises from the uranyl anion, its loss of intensity over time signifies the gradual conversion of the $[UO_2Cl_4]^{2-}$ unit into a relatively nonluminescent species.

As a control experiment, $Cs_2UO_2Cl_4$ was irradiated in the same manner as that for **1**−**3** and displayed a noticeable loss of emissive intensity (~36%). This was surprising given that this is a well-studied complex, and such photoreactivity, to our knowledge, has not previously been described. While at first it seemed that a similar process was in play for $Cs_2UO_2Cl_4$ (as in **1**−**3**), a few significant differences were observed that suggested the mechanisms were dissimilar. First, *all* of the lost emissive intensity (~43%) was recovered after 20 h in darkness in two of three experiments, and nearly all emission intensity returned in the third (Figure S10). This contrasts the partial recovery observed in the viologen-containing species (Figure S9). Second, the excitation profile features no

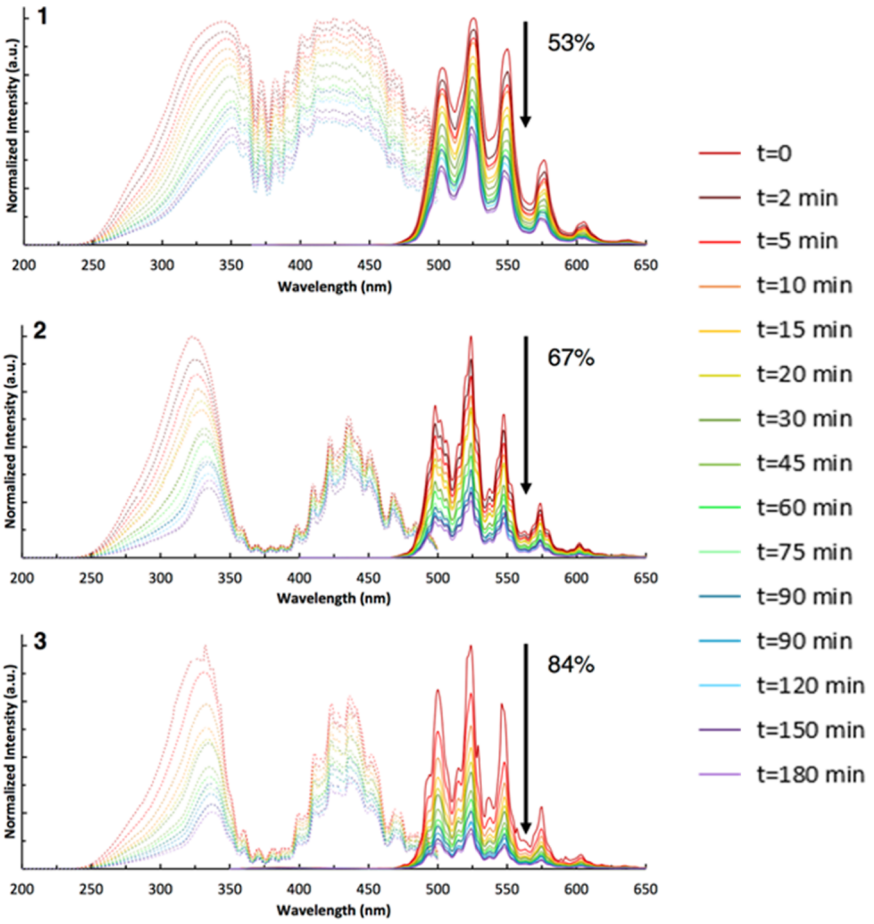

Figure 5. Luminescence spectra of **1**−**3** collected over 3 h at different time intervals following exposure to UV light (345 nm for **1** and 325 nm for **2** and **3**) This shows that the emission intensity is quenched as a function of UV light exposure. Excitation/emission wavelengths for **1**−**3** are 345 nm/526 nm, 325 nm/524 nm, and 325 nm/525 nm, respectively.

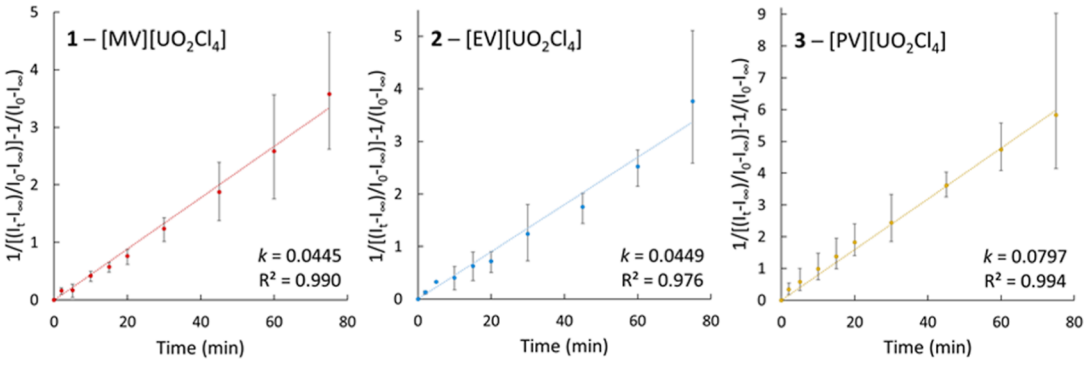

Figure 6. Kinetics of photoinduced emission quenching of **1**−**3**. Emission monitored at 526 nm for **1**, 524 nm for **2**, and 525 nm for **3**.

significant band shifting, and the relative intensity of the bands remains constant, regardless of irradiation time. Finally, the rate of quenching follows a first-order rate law, which is inconsistent with the second-order law(s) observed in **1**−**3** (Figure S11) and suggests that a different mechanism is present versus the viologen compounds.

Electron Paramagnetic Spectroscopy. EPR was utilized to detect the emergence and character of radical species generated by the irradiation of these materials. It is common in solid-state viologen-bearing materials to observe signatures associated with reduced viologen cations at values near to those of free unpaired electrons (*g* factor = 2.002). As such, EPR spectra were collected on **1**−**3** after varying periods of irradiation using a broadband mercury lamp light source.

Before **1**−**3** were irradiated, all the nominally diamagnetic materials displayed features centered at *g*-factors of approximately 2.03 and 2.01. In the case of **1**, the positions of these peaks are consistent with the presence of viologen-centered radicals. The feature at a *g*-tensor of 2.005 and additional features (marked by asterisks in Figure 7) are also seen in the spectra recorded for the methyl viologen chloride hydrate reagent prior to irradiation (Figure S12).[53−56] The final feature at 2.001 is consistent with a long-lived triplet state of a carbon-based aromatic ring. Initial spectra of **2** and **3** show features at

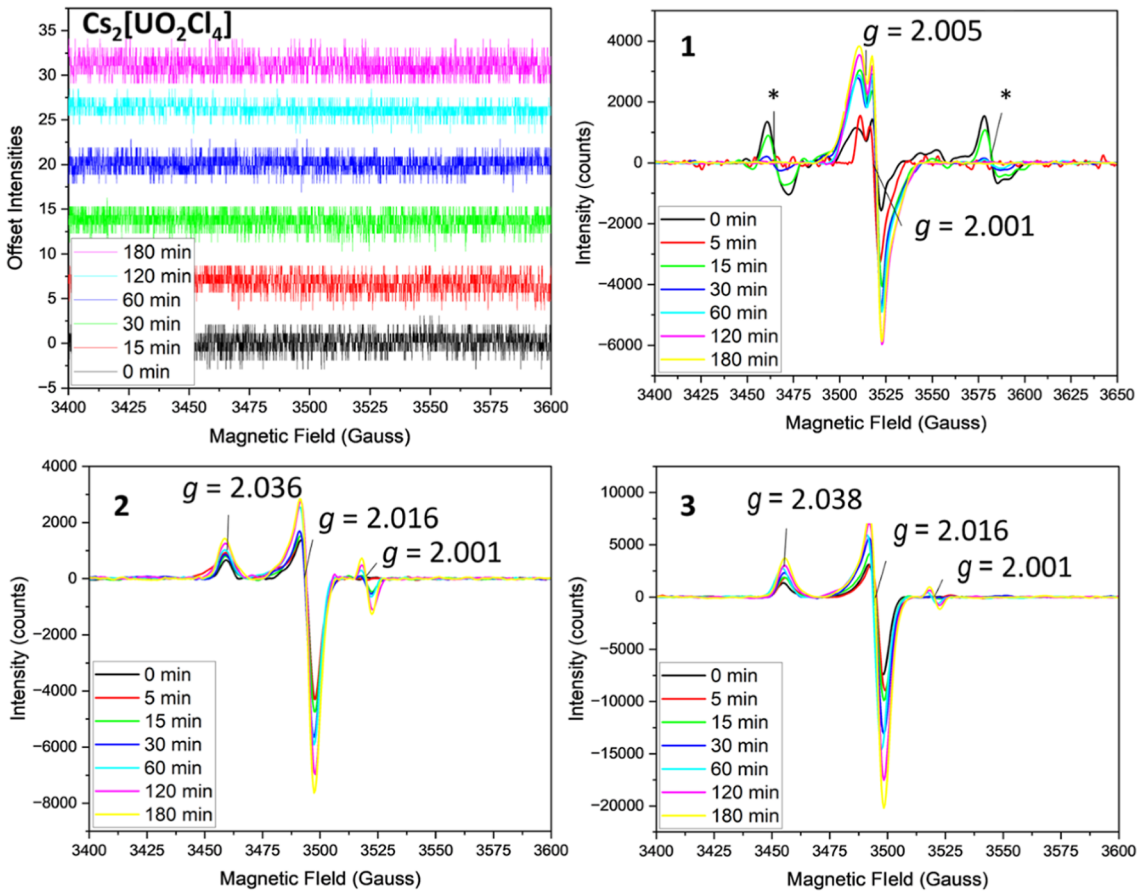

Figure 7. EPR spectra of $Cs_2UO_2Cl_4$ and **1**–**3** after exposure to UV radiation. Asterisks mark the location of peaks also observed in the viologen starting materials (Figure S12).

g-tensors of approximately 2.036–2.038 and 2.016 that align with the previous accounts of paramagnetism in U(VI) complexes.[4,5,8] The profile observed is attributed to axial anisotropy about the uranyl metal center with regard to magnetic moment. In both cases, it is interesting that *any* profile is observed owing to the supposed diamagnetism of U(VI). We conducted additional EPR experiments using $Cs_2UO_2Cl_4$ to establish whether this was a property inherent to $[UO_2Cl_4]^{2-}$ or if it arises owing to the presence of the viologen cation. Interestingly, no signal associated with $[UO_2Cl_4]^{2-}$ could be observed in these experiments, making our finding of baseline paramagnetism in **1**–**3** even more surprising. Though we cannot say with certainty why this is, it is likely due to either the accumulation of stable radical species as the material is exposed to ambient light or the manifestation of temperature-independent paramagnetism [TIP; a known property of U(VI) complexes] that is amplified by the presence and interaction with the viologens. This signal increases as we go from **1** to **2** to **3**. This is consistent with the rate of quenching seen in luminescence experiments, but in minimally irradiated samples, that is to say, the baseline paramagnetism in these materials increases in the same order as luminescence quenching.

The profiles of **1**–**3** undergo distinct changes upon irradiation. All materials see a progressive increase in the features present in the range of g = 2.040 to 2.005 as a function of irradiation; the intensity of the feature after 3 h of irradiation increases from **1** to **2** to **3** (Figure 7). This suggests that the degree of radical generation is increasing as a function of irradiation. Moreover, the degree of radical generation correlates to the degree of quenching observed in luminescence experiments. The material that generated the greatest number of radicals associated with the paramagnetic U(VI) complex observed in this study experienced the greatest reduction of emissive intensity (**3**), and the material with the fewest radicals experienced the least quenching (**1**). This is a key aspect of this study as it is the experimental evidence for the fact that irradiation causes radicalization that is concurrent with emissive quenching, allowing us to probe photoreactivity via magnetic measurements as well as luminescence spectroscopy.

Progressive irradiation also amplifies a signal already present in **1** (g-factor = 2.005) and produces a new signal in **2** and **3** (g-factor = 2.001). These features are consistent with radical viologen species (Figures S12–S14) and N-centered radicals, suggesting some degree of electron transfer from the uranyl species to the viologen.[21,53−55] This process agrees with the viologen literature writ large and is generally confirmed using EPR. However, we note that this feature is relatively minor compared to that of the uranyl metal complex in **2** and **3**; the intensity and the rate of increase of intensity are both greater for the $[UO_2Cl_4]^{2-}$ complex than the viologen species for these two compounds. Similar experiments conducted with $Cs_2UO_2Cl_4$ reveal that no amount of UV irradiation within the same time frame produces *any* signal in the absence of the viologen.

Taken together, this suggests the generation of a viologen cation radical species upon irradiation with UV light that

agrees in part with the previously reported viologen-facilitated PET radicalization schemes. However, a major contributor to the loss of luminescence as a function of irradiation in **2** and **3** appears to be a result of the degree of radicalization of $[UO_2Cl_4]^{2-}$ apart from the viologen. Moreover, the $[UO_2Cl_4]^{2-}$ complex exhibits a state of persistent baseline paramagnetism, prompted by ambient irradiation or TIP, which can be amplified through exposure to UV light. This phenomenon does not occur in the control species, $Cs_2UO_2Cl_4$, and is facilitated by the presence of the viologen chromophore.

Literature Precedence of Uranyl Photoreactivity. The photoreactivity of uranyl-bearing systems has long been observed and is frequently utilized in a variety of contexts.[11,57−60] Typically, the process is related to the phenomenon detailed by Espenson et al., whereby UO_2^{2+} in solution is excited by incident light to form a highly oxidizing UO_2^{2+*} species.[6] This species, in turn, reacts with organic substrates or water, usually via hydrogen abstraction, to create organic radicals and a newly reduced $U(V)O_2^{+}$ species. $U(VI)O_2^{2+}$ is regenerated upon the oxidation of the pentavalent species, either by an organic substrate or molecular oxygen. In the latter case, oxygen can be converted to peroxide in solution, which, as discussed previously, can result in peroxide-bound uranyl species.[3] This is closely related to how the photoreactivity of uranyl heterocatalysts causes C−H bond activation in some substrates.[7] It has also recently been suggested that uranyl heterocatalytic MOFs, with substrate-accessible void space, can photoradicalize and stabilize pentavalent uranium in its structure.[8] We suspect, based on the characterization discussed above, that the quenching in this system is driven primarily by the radicalization of the $[UO_2Cl_4]^{2-}$ complex and amplified by the presence of viologens, which may accept and stabilize radical electrons. However, to investigate the nature of the reacted species, and more pointedly the possibility of U(V) generation, we have employed several methods to identify the changes in properties between the pristine and reacted species.

Probing the Nature of the Reacted Species. Luminescence and EPR studies illustrate that irradiation causes significant changes in these materials such that their properties change over irradiation time. We are interested in probing the nature of the newly reacted species beyond establishing its presence. As such, we have employed various characterization techniques to pristine (i.e., unirradiated) and reacted samples to elucidate the differences between the two species.

SCXRD Analysis. Pristine single crystals of compounds **1** and **2** were isolated and characterized using SCXRD (structural disorder modeling made a similar analysis of **3** prohibitively difficult). The same crystals were then irradiated using a Dymax BlueWave 200 lamp for 2 h, quickly remounted, and a second data set was collected. We then compared the structure of the two data sets to probe for differences in bonding that may have occurred over the course of irradiation. It was clear that there was no phase change or significant changes in unit cell parameters for either material. Moreover, there were no statistically significant changes observed in bond lengths in **1** or **2** when evaluating the structural refinement. It is well established that changes in bonding are common in photoreactive viologen-containing materials; however, no definitive changes in the structure of the viologen, or $[UO_2Cl_4]^{2-}$ for that matter, are observed between the pristine and irradiated samples.

Raman Analysis. Two sets of samples were prepared for the collection of Raman data: one set consists of pristine crystalline samples of **1**−**3**, while another set contained samples that were irradiated with broadband UV/vis light from our Dymax Bluewave 200 light source for 2 h. The Raman spectra for both sets of samples were collected and are reported in the Supporting Information (Figures S12−14). Overall, very little information about the nature of reacted species could be derived. The uranyl anion displays few characteristic features, the most prominent being the O−U−O symmetric stretch centered at about 830 cm^{-1}.[61] We would expect that any electron transfer occurring would disrupt the bonding in the $[UO_2Cl_4]^{2-}$ complex, resulting in shifting, most likely red-shifting corresponding to bond weakening, but in fact there are no discernible shifting in the observed features.[62,63] Moreover, the majority of the profile arises as a result of the viologens, which are also anticipated to respond as dicationic species are converted to monocationic radical species.[64−67] The peak positions change very little in response to radiation, but interestingly many features (especially in the 1000−1400 cm^{-1} region) are diminished relative to the symmetric uranyl stretch. We note this because Poizat et al. observe that the dicationic methyl viologen displays prominent features at 1193 and 1299 cm^{-1} that are not present in the chemically reduced form. Additionally, the radical methyl viologen displays features at 1022, 1038, and 1534 cm^{-1}, which we also see in our irradiated methyl viologen uranyl tetrachloride compound (Figure S15). Whereas some Raman characterization of ethyl viologen and propyl viologen derivatives are reported, little points to the direct detection of radical species.[68,69] We note that the EV and PV analogues show diminished peaks in the 1000−1400 cm^{-1} range and emergence of features for **2** (641, 1359, and 1526 cm^{-1}) and **3** (1022 and 1357 cm^{-1}). It is noteworthy that the positions of the uranyl symmetric stretches do not change upon irradiation, which is consistent with the crystallographically determined U−O bond lengths.

Generation of Radical Species as a Means of Quenching. A recent work by Wang et al. invokes the formation of ligand-based radicals, which disrupt the uranyl electronic transition pathway resulting in emission quenching over long periods of UV irradiation.[9] Generally speaking, these compounds feature conjugated ancillary ligands that experience bond-breaking owing to incident radiation. Subsequent radicals are formed and stabilized by the bound ligands. If we consider an analogous process in **1**−**3**, radicalization would occur between the uranium center and a chloride ligand. This is reminiscent of the previously observed phenomena of equatorial ligand donors participating in LMCT, whereby an electron is transferred from the U−L bonding orbitals to the U 5f orbitals upon excitation.[70] The excited state would be stabilized by the unaffected chloride ligands in the equatorial plane, preventing the immediate reformation of the U−Cl bond and concurrent return to the ground-state electron configuration. The result would be a radical shared among the equatorial ligands that disrupts the frontier orbital electron construct to such a degree that the emission pathway is no longer available and thus quenching occurs.

One may expect that this process is less likely to occur in the $[UO_2Cl_4]^{2-}$ species owing to its diminished capacity to distribute charge when compared to aromatic ligands. Indeed, prolonged irradiation studies conducted on $Cs_2UO_2Cl_4$ speak

to the relative insensitivity of the $[UO_2Cl_4]^{2-}$ anion to radicalization (evidenced by EPR spectroscopy; Figure 7). However, it appears that we have sufficiently perturbed the electronic structure by introducing viologen cations, such that the generation of uranyl radical species in **1−3** is possible using UV radiation shown by the increase in the paramagnetic character as the material is irradiated. Radicalization is a common feature of viologen-bearing materials, as mentioned previously, and is generally accompanied by one electron reduction of the dication. While this appears to be occurring to some extent (discussed below), a surprising degree of UV light-induced radicalization is localized to the $[UO_2Cl_4]^{2-}$ anion. Therefore, while the viologen is being reduced, the presence of the viologen cation increases the propensity of the $[UO_2Cl_4]^{2-}$ anion to radicalize separate from its ability to abstract electrons. We believe this ligand-stabilized radicalization is responsible for the quenching observed in our luminescence studies, similar to that Wang et al. have shown.

This rationalization also allows us to make a few observations about the changes seen in the excitation profiles of these materials between pristine and radicalized species. The radicalization of the $[UO_2Cl_4]^{2-}$ anion is likely tied to LMCT resulting from the excitation of the equatorial chloride ligands. As U−Cl bonding orbitals are depopulated and stabilized in excited states, evidenced by the increased EPR signal, the ability to undergo subsequent LMCT and emission is severely reduced, manifesting as diminished emissive intensity. Moreover, the red-shifting seen in the equatorial excitation band of **1−3** may be a result of destabilization of the U−Cl bond in the radicalized species.

In addition to the generation of metal-centered radicals, EPR measurements also point to a concurrent phenomenon: the generation of radical monocationic viologen species. The observed viologen radical EPR signal requires us to consider the unconventional possibility of electron transfer *from* the uranyl unit (electron-rich) *to* the viologen (electron-poor) ions, facilitated by incident UV light, which may initially be expressed by the equation

$$[UO_2Cl_4]^{2-} + RV^{2+} \rightarrow [UO_2Cl_4]^{1-} + RV^{1+} \quad (1)$$

where RV is a generic viologen species. This process would fit the well-documented electron-accepting ability of viologen materials but requires $[UO_2Cl_4]^{2-}$ to donate electrons. While this departs from general assumptions about how U(VI) can participate in photoreactivity, the electron-withdrawing capability of the viologen coupled with the surprising degree to which uranyl-complex radicals may be present in modestly irradiated materials may speak to this hitherto undescribed possibility, that is, oxidation of the complex anion.

Photoinduced Electron Transfer Mechanism. The study of Ikeda et al. is helpful in describing the dynamics at play that can lead to PET.[71] In the solution state, and our control uranyl tetrachloride species, the excited electron has no pathway of relaxation besides returning to the radicalized chloride, and indeed luminescence studies show that $CsUO_2Cl_4$ will completely relax and return to its original emissive intensity. However, in **1−3,** we have reliable electron reservoirs neighboring the $[UO_2Cl_4]^{2-}$ complex (i.e., the viologen) that could be capable of accepting the excited electron, thereby *oxidizing* the uranyl complex. This would explain the difference in the rate with which emissive intensity returns to $Cs_2UO_2Cl_4$ versus the viologen-bearing materials, as well as the decline in the relative intensity of the high-energy equatorial excitation band (as the equatorial ligands are deprived of electrons). Moreover, it would also follow that if the viologen species were changed, the electron-accepting capability or radical stability of the viologen would alter the rate of quenching.

Bearing this proposed photoreactivity scheme in mind, we initially proposed a derivative of Wang's mechanism by the following elementary steps

$$[UO_2Cl_4]^{2-} + h\nu \rightarrow {}^*[UO_2Cl_4]^{2-} \quad \text{uranylexcitation} \quad (2)$$

$${}^*[UO_2Cl_4]^{2-} + RV^{2+} \rightarrow \{{}^*[UO_2Cl_4]^{2-}\cdots RV^{2+}\} \quad \text{complexation} \quad (3)$$

$$\{{}^*[UO_2Cl_4]^{2-}\cdots RV^{2+}\} \rightarrow [UO_2Cl_4]^{1-} + RV^{1+} \quad \text{electrontransfer} \quad (4)$$

Considering this scheme, stepwise, from an electronic perspective, we have initial excitation of the uranyl unit from a singlet ground state to an excited triplet state. It is worth noting that this process is the product of charge transfer from bonding orbitals, mostly chloride ligand in character, to the U 5f orbitals.[47] Once promoted, the excited electron would be transferred to the vacant viologen π^* orbital which would lead to an interaction between the excited $[UO_2Cl_4]^{2-}$ unit and the viologen. Once the interaction ceases, the excited electron of uranium (originally from the uranyl ligands) would be transferred to the viologen, creating a new monocationic doublet viologen species and an oxidized monoanionic $[UO_2Cl_4]^{-}$ complex. The nontrivial process of formal electron transfer across molecular fragments would set this photochemical process apart from those previously documented for radical-forming solid uranyl materials (this process is illustrated in Figure 8). This scheme would explain the reactivity seen in

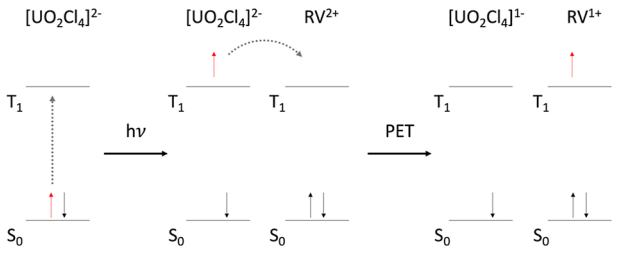

Figure 8. Simplified diagram describing the excitation and subsequent transfer of one electron from the uranyl species to the viologen molecule via photoinduced electron transfer. S_0, singlet ground state; S_1, first excited state; T_1, first triplet state; PET, photoinduced electron transfer.

this system and is in agreement with the characterization of the reacted species, i.e., EPR signal and the changes in excitation profile. To further characterize the nature of this reactivity and the specific pathways by which it may proceed, additional experimentation, such as transient absorption spectroscopy, must be done following this study.

Criteria for Electron Transfer. For this process to be viable, the properties of the materials must satisfy certain conditions: (i) the process must be thermodynamically favorable and (ii) electronic structure and excited-state transitions must serve as pathways to electron transfer. We probed these two criteria using a hybrid experimental and

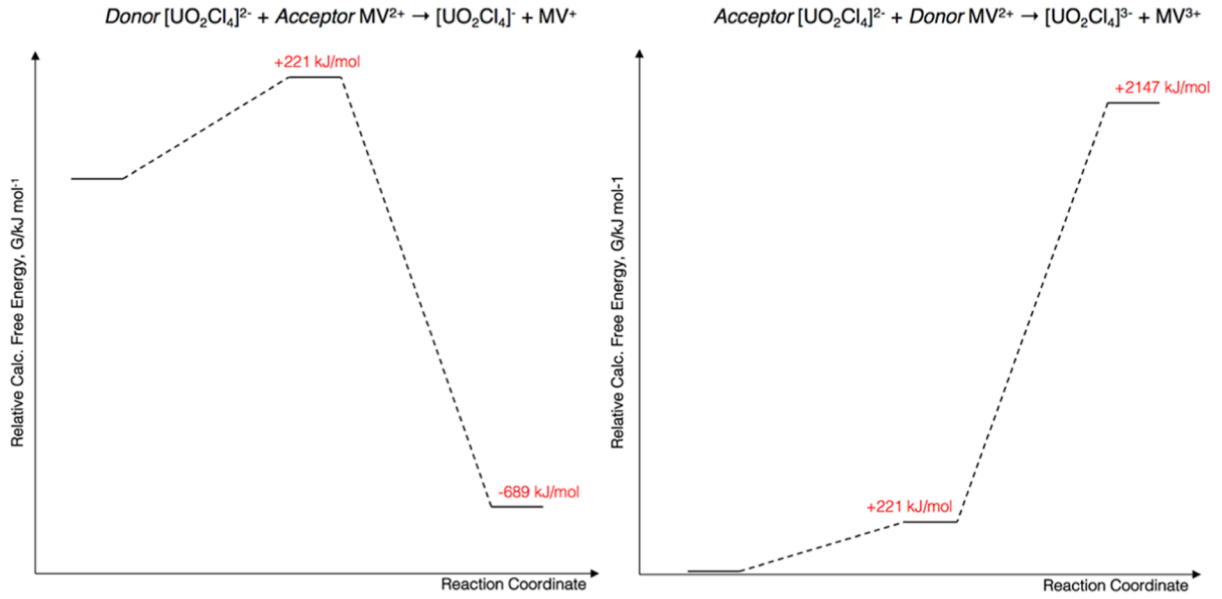

Figure 9. DFT-calculated reaction coordinate diagram showing changes in free energy for the stepwise transfer of one electron between $[UO_2Cl_4]^{2-}$ and MV^{2+}. The numbers listed above each energy level refer to the relative change in free energy in kJ mol^{-1} vs the reactants.

computational approach. Experimentally, we employed EPR spectroscopy to directly measure the emergence of radical species (discussed above) and the Rehm–Weller equation to determine the thermodynamic likelihood based on the energy of light being absorbed by the material and the reduction potentials of the relevant species. Computationally, density of states calculations allowed us to determine the band structure of the materials in order to evaluate whether an electronic structure that is amenable to electron transfer from the U 5f orbitals to the viologen π^* orbitals is present. We also carried out free-energy change and TD-DFT calculations to reinforce our experimental thermodynamic data and calculated the origin and destination of electronic transitions that would be relevant to electron transfer. With these data, we validate the possibility of an oxidized $[UO_2Cl_4]^-$ species in these materials.

Rehm–Weller Analysis. To assess the thermodynamic favorability associated with electron transfer from uranyl tetrachloride to the corresponding viologen species, a Rehm–Weller analysis was conducted using the equation

$$\Delta G_{ET} = (E_{ox} - E_{red}) - E_s - \frac{e_s^2}{\varepsilon_a}$$

The Rehm–Weller equation describes the relationship between the reduction potentials of the redox pair involved in electron transfer (E_{ox}, E_{red}), the ground-state singlet energy of the complex (E_s), and the subsequent Coulombic attraction the pair experience as a result of the reaction (e_o^2/ε_a = 0.15 eV).[72] Standard reduction potentials of the viologen dications have been obtained via cyclic voltammetry at −0.582, −0.628, and −0.620 V for methyl, ethyl, and propyl viologens, respectively. While an oxidation potential for $[UO_2Cl_4]^{2-}$ is unreported, we may instead use the potential associated with the oxidation of the chloride ligands (−1.3583 V), assuming no overall change in the oxidation state of the UO_2^{2+} ion.[73] The E_s values are calculated based on the absorption edge of these materials, which are derived from the DRS spectra. Rehm–Weller parameters are provided in Table S4 (Supporting Information), with the calculated ΔG values of −3.37, −3.06, and −2.98 eV for **1**, **2**, and **3**, respectively. The analysis confirms that the photochemical reaction of a photoexcited electron transfer from the $[UO_2Cl_4]^{2-}$ anion to the viologen cation has a negative ΔG value in all cases and thus is thermodynamically favorable. This analysis supports our reaction mechanism described above in that the $[UO_2Cl_4]^{2-}$ unit acts as a photoexcited electron *donor* to generate a reduced viologen cation and oxidized $[UO_2Cl_4]^-$ ion.

Changes in Free Energy (ΔE kJ mol^{-1}). As initially indicated by the Rehm–Weller analysis, the transfer of an electron from $[UO_2Cl_4]^{2-}$ to the viologen species occurs as a thermodynamically favorable reaction. To validate further, we have calculated the reaction energies of the $[UO_2Cl_4]^{2-}$ and viologen units in various oxidation states using DFT (Table S5). The change in energy from the *singlet* dianionic $[UO_2Cl_4]^{2-}$ to the *triplet* $[UO_2Cl_4]^{2-}$ or *doublet* $[UO_2Cl_4]^{1-}$ species is positive/endothermic for both charges/spins. The greatest change in energy (+221 kJ/mol) occurs as the $[UO_2Cl_4]^{2-}$ unit electronically rearranges from the singlet to the triplet state. Notably, the doublet state or oxidized $[UO_2Cl_4]^-$ species is *lower* in energy compared to the triplet state (by −40.3 kJ/mol), indicating the propensity to act as a potential metastable state upon oxidation. The corresponding changes in energy for the reduction of RV^{2+} to RV^+ are distinctly negative/exothermic and are greater in magnitude (852–869 kJ/mol) compared to the $[UO_2Cl_4]^{2-}$ species. ΔE for the reduction of the viologen species is on the order of $MV^{2+} > EV^{2+} \gg PV^{2+}$. Using the ΔE values, we have calculated the free-energy change of the reaction involving the redox of $[UO_2Cl_4]^{2-}$ and the viologen dication where the $[UO_2Cl_4]^{2-}$ unit acts as an electron donor in Figure 9. Clearly, the overall reaction is energetically *favorable* where the oxidized $[UO_2Cl_4]^-$ and reduced RV^+ products are significantly lower in energy compared to the reactant species, and the photoexcitation of the $[UO_2Cl_4]^{2-}$ triplet is the activation barrier. This change in free energy supports the Rehm–Weller assertion that the photoexcited triplet $[UO_2Cl_4]^{2-}$ is capable of transferring an electron to the viologen dication. Importantly, these calculations do not invoke a U(V) center and instead support the formation of a radicalized $[UO_2Cl_4]^-$ species,

whereby the unpaired electron is delocalized across the O/Cl ligands (Table S6).

Free-energy evaluation also requires considering the alternative reaction where $[UO_2Cl_4]^{2-}$ acts as an electron *acceptor* and the viologen as an electron *donor*. Whereas the removal of an electron from the uranyl species has ΔE lower than that of the triplet state, the reduced $[UO_2Cl_4]^{3-}$ species (also a doublet) is significantly higher in energy than the triplet state (by +281 kJ/mol). Furthermore, oxidization of the viologen to produce a tricationic species is positive in energy and greater by an entire order of magnitude. The reaction coordinates demonstrate that this reaction, where $[UO_2Cl_4]^{2-}$ is the electron acceptor, is energetically *unfavorable*.

Band Structure. Common to the reduction of viologens in photoreactive materials, and PET more generally, is the presence of energetically accessible π^* molecular orbitals into the band structure, which may act as photoexcited electron acceptors. Excitation of the $[UO_2Cl_4]^{2-}$ unit and the subsequent capture of photoexcited electrons via viologen π^* acceptors, as mentioned above, would constitute a formal electron charge-transfer mechanism between ion pairs. Ideally, for efficient electron transfer in this system, the π^* acceptor orbitals should be energetically close to those of U 5f which serves as the lowest excited triplet state for the $[UO_2Cl_4]^{2-*}$ ion. To probe whether such conditions exist in these materials, we have mapped the band structure of **1**−**3** as well as $[UO_2Cl_4]^{2-}$, and the calculated total and partial density of states of **1**−**3** are shown in Figure 10.

In the absence of viologen cations, the $[UO_2Cl_4]^{2-}$ valence band is composed of the Cl p-states, whereas the conduction band is composed of the empty U 5f atomic orbitals. This band structure is typical of uranyl-containing compounds and has been documented previously.[47] The introduction of viologen cations inserts π^* molecular orbitals which, in terms of energy, lie below U 5f. This orbital construct is consistent with the isodensity renderings of the frontier orbitals (Figure 10), where the HOMO and HOMO − 1 are dominantly Cl p in character with a minor O p contribution to the HOMO − 1, while the LUMO and LUMO + 1 are energetically degenerate π^* orbitals that reside on the viologen cations. Such a band structure is ideal for formal electron transfer from the $[UO_2Cl_4]^{2-}$ anion to the viologen cations, as the population of π^* may act as the lowest possible triplet state. The π^* energy decreases on the order of $MV^{2+} > EV^{2+} > PV^{2+}$. The conduction band of **3** is of note as the *filled* π orbitals of PV^{2+} are higher than the Cl p-states of $[UO_2Cl_4]^{2-}$, making the frontier orbitals strictly viologen in origin.

Calculated Electron Transitions. Time-dependent density functional theory calculations were carried out to ascertain the electronic transitions in **1**−**3** upon UV irradiation at the high-energy (equatorial ligand) excitation band (345 for **1** or 325 nm for **2** and **3**) and provide insights into the photochemical mechanism responsible for the loss of uranyl emission intensity. For compound **1**, an energetically relevant singlet excited state is calculated at 359 nm with a strong oscillation value ($f = 0.0187$). Isodensity representations of the dominant molecular orbitals involved in this excited-state transition are shown in Figure 11. Renderings of all molecular orbital transitions for this exited state are included in the Supporting Information. The dominant TD-DFT transitions at 359 nm for the singlet state can be described as a rearrangement of electrons about the $[UO_2Cl_4]^{2-}$ unit. Here, electrons originating from the HOMO/HOMO − 2, which is a mixture

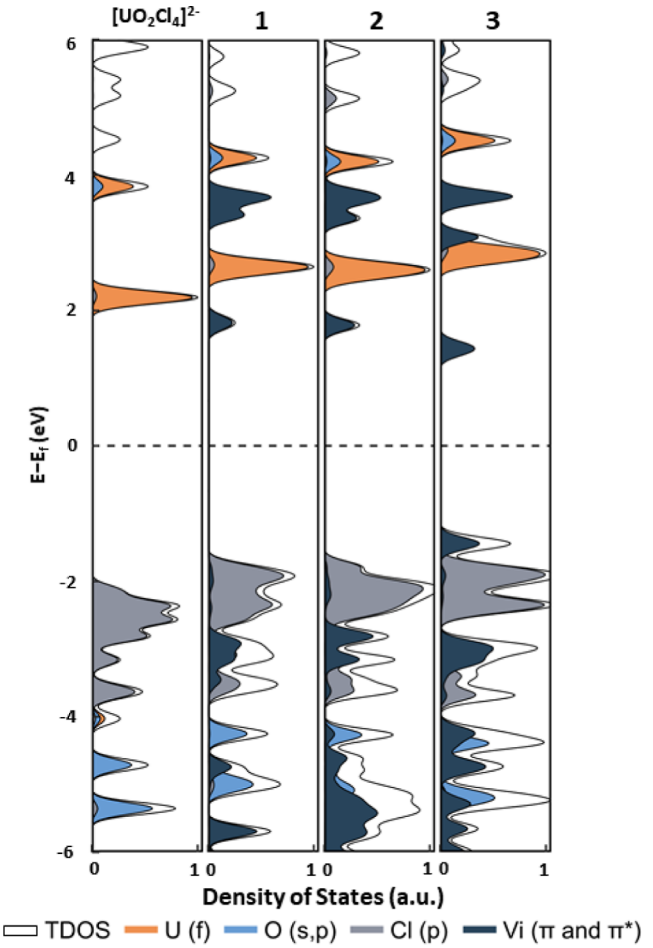

Figure 10. Total density of states of $[UO_2Cl_4]^{2-}$ and **1**−**3** and partial density of states projected onto the atomic orbitals of U, O, and Cl atoms and the molecular orbitals (π and π^*) of viologen cations. The conduction band of $[UO_2Cl_4]^{2-}$ (orange) is U 5f in character, in agreement with Denning, but each of **1**−**3** shows that a viologen π^* state (dark blue) has been introduced into the band structure. This new band is lower in energy than the U 5f orbital and may allow for the population of viologen π^* orbitals by the electrons from the $[UO_2Cl_4]^{2-}$ anion. The Fermi level is shown as a dashed black line.

of O p- and/or Cl p-states, are populated into empty U 5f atomic orbitals (shown in Figure 12). As mentioned previously, this electronic behavior is typical of uranyl complexes, including $[UO_2Cl_4]^{2-}$.

Of interest is the TD-DFT analysis of the degenerate triplet states at 438 nm, which corresponds to the experimental excitation peak at 436 nm. Isodensity representations for orbital transitions at this energy are distinctly different from those of the previous singlet state. As shown in Figure 13, acceptor orbitals for the 438 nm triplet state are the LUMO + 1 and LUMO + 2 and are solely composed of the π^* orbitals of the MV^{2+} dication. Importantly, this triplet state is lower in energy than that of the singlet state achieved via UV irradiation and thus energetically accessible. The TD-DFT findings, while supporting the electron transfer between ion pairs, indicate two important points: (i) initial irradiation at 350 nm leads to a singlet O/Cl p → U 5f transition and (ii) this singlet state decays to a lower-energy triplet state which resides on MV^{2+}, constituting an electron transfer from the excited state $[UO_2Cl_4]^{2-}$ anion. TD-DFT analysis of compounds **2** and **3**

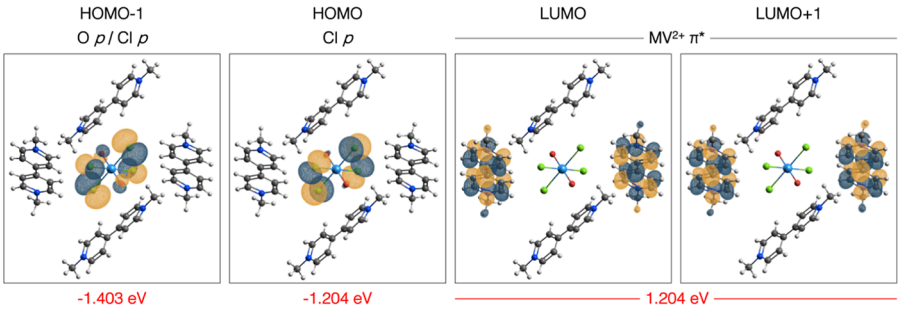

Figure 11. Isodensity representations of frontier molecular orbitals (HOMO − 1 to LUMO + 1) calculated for **1**. Orbital assignment is provided above, while energy levels are marked in red below. Note that the LUMO and LUMO + 1 at 1.204 eV are degenerate.

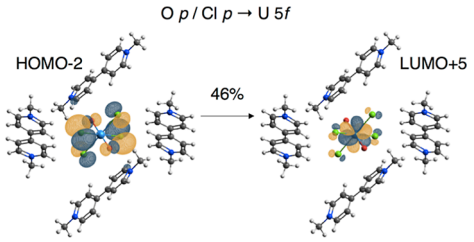

Figure 12. TD-DFT isodensity representations of dominant molecular orbitals in **1** involved in electronic transitions for the *singlet* state at 359 nm. A total of 85% of the pathways are O p/Cl p → U 5f transition in nature.

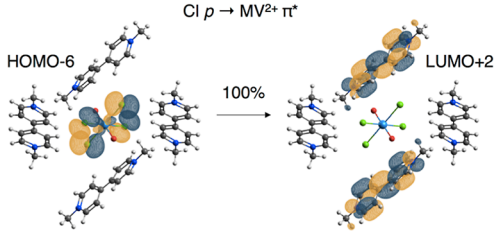

Figure 13. TD-DFT isodensity representations of molecular orbitals in **1** involved in electronic transitions for the *triplet* state at 438 nm. This pathway is a Cl p → U 5f transition.

provide nearly identical results, implying that this mechanism holds for all three uranyl viologen compounds.

CONCLUSIONS

We describe the synthesis, characterization, and kinetic study of three novel photoreactive uranium-based materials, featuring $[UO_2Cl_4]^{2-}$ and various alkylated viologens. These materials exhibit photoreactivity in the form of progressive loss of emissive intensity when exposed to UV light. EPR measurements suggest two concurrent phenomena: $[UO_2Cl_4]^{2-}$ radicalization and PET to the viologen cation. The identity and interaction with the viologen had a critical role in the rate at and degree to which these processes occur, evident in both luminescence and EPR studies. A scheme describing formal electron transfer from the $[UO_2Cl_4]^{2-}$ unit to the viologen is detailed and supported by various experimental and computational analyses. Our hybrid experimental and computational approach demonstrates the thermodynamic favorability and proper band structure and excitation pathways for the photoinduced oxidization of $[UO_2Cl_4]^{2-}$ and the subsequent reduction of the viologen ions. Additional findings established that $Cs_2UO_2Cl_4$ displayed no radicalization upon irradiation and that the radicalization observed in **1**−**3** must arise from the presence of viologens. Interestingly, $Cs_2UO_2Cl_4$ displays the modest reversible emissive quenching upon exposure to UV light, but the cause is not immediately clear from this study.

To our knowledge, this is the first report of a photogenerated, solid-state, air-stable $[UO_2Cl_4]^{2-}$ radical. As such, our findings demonstrate a suitable methodology for the study of novel solid-state radical uranyl species with implications for f-orbital participation in bonding. Since this radicalization seems to persist over long periods of time, it provides the opportunity to investigate the effect this new activity has on the bonding and reactivity of these compounds. In future studies, we plan to investigate what role ligands play in the photoreactivity of solid-state uranyl materials considering the propensity of UO_2^{2+} to form several closely related anions (i.e., $[UO_2Br_4]^{2-}$, $[UO_2SCN_5]^{3-}$, etc.). Our findings have significant implications toward the study of uranyl chemistry writ large, including the use of the uranyl unit as a photocatalyst, and improving our fundamental understanding of the photochemical mechanisms afforded by its incorporation into new functional materials. Moreover, this may be a phenomenon that can be repeated with other redox-active f-block elements which, in turn, may reveal novel information as to the bonding and reactivity of the transuranic elements.

ASSOCIATED CONTENT

Powder X-ray diffraction patterns, additional DFT calculations, Tauc plots, additional luminescence spectra and kinetic data, EPR and Raman spectra, voltammograms, and Rehm−Weller analysis. X-ray data for compound 1 pre- and post-irradiation (1−−pristine and 1−−irradiated, respectively) and X-ray data for compound 2 pre- and post-irradiation (2−−pristine and 2−−irradiated, respectively) (PDF)

Accession Codes

CCDC 2118265−2118267 contain the supplementary crystallographic data for this paper. These data can be obtained free of charge via www.ccdc.cam.ac.uk/data_request/cif, or by emailing data_request@ccdc.cam.ac.uk, or by contacting The Cambridge Crystallographic Data Centre, 12 Union Road, Cambridge CB2 1EZ, UK; fax: +44 1223 336033.

AUTHOR INFORMATION

Corresponding Author

Christopher L. Cahill − *Department of Chemistry, The George Washington University, Washington, District of*

Columbia 20052, United States; orcid.org/0000-0002-2015-3595; Email: cahill@gwu.edu

Authors

Jordan A. Herder − *Department of Chemistry, The George Washington University, Washington, District of Columbia 20052, United States;* orcid.org/0000-0003-2355-1457

Samantha J. Kruse − *Department of Chemistry, University of Iowa, Iowa City, Iowa 55242, United States*

Aaron D. Nicholas − *Department of Chemistry, The George Washington University, Washington, District of Columbia 20052, United States; Pacific Northwest National Laboratory, Richland, Washington 99354, United States*

Tori Z. Forbes − *Department of Chemistry, University of Iowa, Iowa City, Iowa 55242, United States;* orcid.org/0000-0002-5234-8127

Eric D. Walter − *Pacific Northwest National Laboratory, Richland, Washington 99354, United States;* orcid.org/0000-0003-3644-5514

Herman Cho − *Pacific Northwest National Laboratory, Richland, Washington 99354, United States;* orcid.org/0000-0001-7072-2306

Notes

The authors declare no competing financial interest.

■ ACKNOWLEDGMENTS

This work was supported by the U.S. Department of Energy Office of Science, Office of Basic Energy Sciences, Division of Chemical Sciences, Geosciences, and Biosciences, Heavy Element Chemistry program under grant DE-FG02-05ER15736 at The George Washington University. We thank Prof. Raymond J. Butcher (Howard University) for his assistance in the crystallographic modeling of our compounds and Prof. Karah Knope and Alexander Marwitz (Georgetown University) for the use of Raman equipment. We would also like to thank the University of Iowa Free Radical and Radiation Biology Program for the use of EPR equipment. EPR spectroscopic experiments at PNNL were supported by the U.S. Department of Energy Office of Science, Office of Basic Energy Sciences, Division of Chemical Sciences, Geosciences and Biosciences, Heavy Element Chemistry Program, FWP 73200.

■ REFERENCES

(1) West, J. G.; Bedell, T. A.; Sorensen, E. J. The Uranyl Cation as a Visible Light Photocatalyst for C(Sp 3)-H Fluorination. *Angew. Chem.* **2016**, *128* (31), 9069−9073.

(2) Wu, L.; Cao, X.; Chen, X.; Fang, W.; Dolg, M. Photokatalyse der C(sp^3)-H-Fluorierung durch Uranyl mit sichtbarem Licht: Einblicke in den Mechanismus. *Angew. Chem.* **2018**, *130* (36), 11986−11990.

(3) Thangavelu, S. G.; Cahill, C. L. Uranyl-Promoted Peroxide Generation: Synthesis and Characterization of Three Uranyl Peroxo [(UO2)2(O2)] Complexes. *Inorg. Chem.* **2015**, *54* (9), 4208−4221.

(4) Liu, W.; Dai, X.; Xie, J.; Silver, M. A.; Zhang, D.; Wang, Y.; Cai, Y.; Diwu, J.; Wang, J.; Zhou, R.; Chai, Z.; Wang, S. Highly Sensitive Detection of UV Radiation Using a Uranium Coordination Polymer. *ACS Appl. Mater. Interfaces* **2018**, *10* (5), 4844−4850.

(5) Xie, J.; Hou, H.; Lu, H.; Lu, F.; Liu, W.; Wang, X.; Cheng, L.; Zhang, Y.; Wang, Y.; Wang, Y.; Diwu, J.; Hu, B.; Chai, Z.; Wang, S. Photochromic Uranyl-Based Coordination Polymer for Quantitative and On-Site Detection of UV Radiation Dose. *Inorg. Chem.* **2023**, *62* (39), 15834−15841.

(6) Wang, W.-D.; Bakac, A.; Espenson, J. H. Uranium(VI)-Catalyzed Photooxidation of Hydrocarbons with Molecular Oxygen. *Inorg. Chem.* **1995**, *34* (24), 6034−6039.

(7) Wang, K. X.; Chen, J. S. Extended Structures and Physicochemical Properties of Uranyl-Organic Compounds. *Acc. Chem. Res.* **2011**, *44* (7), 531−540.

(8) Zhang, X.; Li, P.; Krzyaniak, M.; Knapp, J.; Wasielewski, M. R.; Farha, O. K. Stabilization of Photocatalytically Active Uranyl Species in a Uranyl - Organic Framework for Heterogeneous Alkane Fluorination Driven by Visible Light. *Inorg. Chem.* **2020**, *59* (23), 16795−16798.

(9) Xie, J.; Wang, Y.; Liu, W.; Yin, X.; Chen, L.; Zou, Y.; Diwu, J.; Chai, Z.; Albrecht-Schmitt, T. E.; Liu, G.; Wang, S. Highly Sensitive Detection of Ionizing Radiations by a Photoluminescent Uranyl Organic Framework. *Angew. Chem.* **2017**, *129* (26), 7608−7612.

(10) Wang, Y.; Yin, X.; Liu, W.; Xie, J.; Chen, J.; Silver, M. A.; Sheng, D.; Chen, L.; Diwu, J.; Liu, N.; Chai, Z.; Albrecht-Schmitt, T. E.; Wang, S. Emergence of Uranium as a Distinct Metal Center for Building Intrinsic X-Ray Scintillators. *Angew. Chem., Int. Ed.* **2018**, *57* (26), 7883−7887.

(11) Nieweg, J. A.; Lemma, K.; Trewyn, B. G.; Lin, V. S. Y.; Bakac, A. Mesoporous Silica-Supported Uranyl: Synthesis and Photoreactivity. *Inorg. Chem.* **2005**, *44* (16), 5641−5648.

(12) Andrews, M. B.; Cahill, C. L. Utilizing Hydrogen Bonds and Halogen-Halogen Interactions in the Design of Uranyl Hybrid Materials. *Dalton Trans.* **2012**, *41* (14), 3911−3914.

(13) Deifel, N. P.; Cahill, C. L. The Uranyl Tetrachloride Anion as a Tecton in the Assembly of U(VI) Hybrid Materials. *CrystEngComm* **2009**, *11* (12), 2739−2744.

(14) Surbella, R. G.; Andrews, M. B.; Cahill, C. L. Self-assembly of [UO2X4]2− (X=Cl, Br) dianions with γ substituted pyridinium cations: Structural systematics and fluorescence properties. *J. Solid State Chem.* **2016**, *236*, 257−271.

(15) Ashton, P. R.; Brown, C. L.; Chrystal, E. J. T.; Goodnow, T.; Kaifer, A. E.; Parry, K. P.; Philp, D.; Slawin, A. M. Z.; Spencer, N.; Stoddart, J. F.; Williams, D. J. The Self-Assembly of a Highly Ordered [2]Catenane. *J. Chem. Soc., Chem. Commun.* **1991**, *9*, 634−639.

(16) Wang, Y.; Frasconi, M.; Stoddart, J. F. Introducing Stable Radicals into Molecular Machines. *ACS Cent. Sci.* **2017**, *3* (9), 927−935.

(17) Li, H. Y.; Xu, J.; Li, L. K.; Du, X. S.; Li, F. A.; Xu, H.; Zang, S. Q. Photochromic Properties of a Series of Zinc(II)-Viologen Complexes with Structural Regulation by Anions. *Cryst. Growth Des.* **2017**, *17* (12), 6311−6319.

(18) Qiu, X. T.; Shi, Q.; Zhang, D. Q.; Lin, Q. F.; Sun, Y. Q. A Multi-Responsive Cd-Viologen Complex: Photochromism, Photomodulated Fluorescence, and Luminescent Sensing. *ChemistrySelect* **2018**, *3* (23), 6611−6616.

(19) Li, M. H.; You, M. H.; Lin, M. J. Photochromism and Photomagnetism in Three Cyano-Bridged 3d-4f Heterobimetallic Viologen Frameworks. *Dalton Trans.* **2021**, *50* (14), 4959−4966.

(20) Li, L. K.; Li, H. Y.; Li, T.; Quan, L. H.; Xu, J.; Li, F. A.; Zang, S. Q. Photochromic and Photomodulated Luminescence Properties of Two Metal-Viologen Complexes Constructed by a Tetracarboxylate-Anchored Bipyridinium-Based Ligand. *CrystEngComm* **2018**, *20* (41), 6412−6419.

(21) Wang, Y.-W.; Li, M.-H.; Zhang, S.-Q.; Fang, X.; Lin, M.-J. Photochromic and Photocontrolled Luminescent Rare-Earth D-A Hybrid Crystals Based on Rigid Viologen Acceptors. *CrystEngComm* **2021**, *23* (36), 6267−6275.

(22) Zeng, L. W.; Hu, K. Q.; Mei, L.; Li, F. Z.; Huang, Z. W.; An, S. W.; Chai, Z. F.; Shi, W. Q. Structural Diversity of Bipyridinium-Based Uranyl Coordination Polymers: Synthesis, Characterization, and Ion-Exchange Application. *Inorg. Chem.* **2019**, *58* (20), 14075−14084.

(23) Li, H. H.; Zeng, X. H.; Wu, H. Y.; Jie, X.; Zheng, S. T.; Chen, Z. R. Incorporating Guest Molecules into Honeycomb Structures Constructed from Uranium(vi)-Polycarboxylates: Structural Diver-

sities and Photocatalytic Activities for the Degradation of Organic Dye. *Cryst. Growth Des.* **2015**, *15* (1), 10−13.
(24) Hu, K.-Q.; Wu, Q.-Y.; Mei, L.; Zhang, X.-L.; Ma, L.; Song, G.; Chen, D.-Y.; Wang, Y.-T.; Chai, Z.-F.; Shi, W.-Q. Novel Viologen Derivative Based Uranyl Coordination Polymers Featuring Photochromic Behaviors. *Chem.—Eur. J.* **2017**, *23* (71), 18074−18083.
(25) Eckert, N. A.; Krause Bauer, J. A.; Connick, W. B. N, N ’-Diethyl-4,4’-Bipyridinium Diiodide. *Acta Crystallogr. C* **1999**, *55* (9), IUC9900101.
(26) Sheldrick, G. M. A Short History of SHELX. *Acta Crystallogr., Sect. A: Found. Crystallogr.* **2008**, *64*, 112−122.
(27) Hübschle, C. B.; Sheldrick, G. M.; Dittrich, B. ShelXle: A Qt Graphical User Interface for SHELXL. *J. Appl. Crystallogr.* **2011**, *44* (6), 1281−1284.
(28) Match!-Phase Analysis using Powder Diffraction, Crystal Impact-Dr. H. Putz & Dr. K. Brandenburg GbR, Kreuzherrenstr. 102, 53227 Bonn, Germany. https://www.crystalimpact.de/match, accessed Oct. 29, 2021.
(29) Frisch, M. J.; Trucks, G. W.; Schlegel, H. B.; Scuseria, G. E.; Robb, M. A.; Cheeseman, J. R.; Scalmani, G.; Barone, V.; Petersson, G. A.; Nakatsuji, H.; Li, X.; Caricato, M.; Marenich, A. V.; Bloino, J.; Janesko, B. G.; Gomperts, R.; Mennucci, B.; Hratchian, H. P.; Ortiz, J. V.; Izmaylov, A. F.; Sonnenberg, J. L.; Williams-Young, D.; Ding, F.; Lipparini, F.; Egidi, F.; Goings, J.; Peng, B.; Petrone, A.; Henderson, T.; Ranasinghe, D.; Zakrzewski, V. G.; Gao, J.; Rega, N.; Zheng, G.; Liang, W.; Hada, M.; Ehara, M.; Toyota, K.; Fukuda, R.; Hasegawa, J.; Ishida, M.; Nakajima, T.; Honda, Y.; Kitao, O.; Nakai, H.; Vreven, T.; Throssell, K.; Montgomery, J. A.; Peralta, J. E.; Ogliaro, F.; Bearpark, M. J.; Heyd, J. J.; Brothers, E. N.; Kudin, K. N.; Staroverov, V. N.; Keith, T. A.; Kobayashi, R.; Normand, J.; Raghavachari, K.; Rendell, A. P.; Burant, J. C.; Iyengar, S. S.; Tomasi, J.; Cossi, M.; Millam, J. M.; Klene, M.; Adamo, C.; Cammi, R.; Ochterski, J. W.; Martin, R. L.; Morokuma, K.; Farkas, O.; Foresman, J. B.; Fox, D. J. *Gaussian 16*, Revision C.01; Gaussian, Inc.: Wallingford CT, 2016.
(30) Becke, A. D. Density Functional Thermochemistry. III. The Role of Exact Exchange. *J. Chem. Phys.* **1993**, *98* (7), 5648−5652.
(31) Lee, C.; Yang, W.; Parr, R. G. Development of the Colle-Salvetti Correlation-Energy Formula into a Functional of the Electron Density. *Phys. Rev. B: Condens. Matter Mater. Phys.* **1988**, *37* (2), 785−789.
(32) Weigend, F.; Ahlrichs, R. Balanced Basis Sets of Split Valence, Triple Zeta Valence and Quadruple Zeta Valence Quality for H to Rn: Design and Assessment of Accuracy. *Phys. Chem. Chem. Phys.* **2005**, *7* (18), 3297.
(33) Krishnan, R.; Binkley, J. S.; Seeger, R.; Pople, J. A. Self consistent Molecular Orbital Methods. XX. A Basis Set for Correlated Wave Functions. *J. Chem. Phys.* **1980**, *72* (1), 650−654.
(34) Küchle, W.; Dolg, M.; Stoll, H.; Preuss, H. Energy adjusted Pseudopotentials for the Actinides. Parameter Sets and Test Calculations for Thorium and Thorium Monoxide. *J. Chem. Phys.* **1994**, *100* (10), 7535−7542.
(35) Cao, X.; Dolg, M. Segmented Contraction Scheme for Small-Core Actinide Pseudopotential Basis Sets. *J. Mol. Struct.: THEOCHEM* **2004**, *673* (1−3), 203−209.
(36) Cao, X.; Dolg, M.; Stoll, H. Valence Basis Sets for Relativistic Energy-Consistent Small-Core Actinide Pseudopotentials. *J. Chem. Phys.* **2003**, *118* (2), 487−496.
(37) Hanwell, M. D.; Curtis, D. E.; Lonie, D. C.; Vandermeersch, T.; Zurek, E.; Hutchison, G. R. Avogadro: An Advanced Semantic Chemical Editor, Visualization, and Analysis Platform. *J. Cheminf.* **2012**, *4* (1), 17.
(38) Heyd, J.; Scuseria, G. E. Efficient Hybrid Density Functional Calculations in Solids: Assessment of the Heyd-Scuseria-Ernzerhof Screened Coulomb Hybrid Functional. *J. Chem. Phys.* **2004**, *121* (3), 1187−1192.
(39) Heyd, J.; Scuseria, G. E. Assessment and Validation of a Screened Coulomb Hybrid Density Functional. *J. Chem. Phys.* **2004**, *120* (16), 7274−7280.
(40) Heyd, J.; Peralta, J. E.; Scuseria, G. E.; Martin, R. L. Energy Band Gaps and Lattice Parameters Evaluated with the Heyd-Scuseria-Ernzerhof Screened Hybrid Functional. *J. Chem. Phys.* **2005**, *123* (17), 174101.
(41) Henderson, T. M.; Izmaylov, A. F.; Scalmani, G.; Scuseria, G. E. Can Short-Range Hybrids Describe Long-Range-Dependent Properties? *J. Chem. Phys.* **2009**, *131* (4), 044108.
(42) Izmaylov, A. F.; Scuseria, G. E.; Frisch, M. J. Efficient Evaluation of Short-Range Hartree-Fock Exchange in Large Molecules and Periodic Systems. *J. Chem. Phys.* **2006**, *125* (10), 104103.
(43) Krukau, A. V.; Vydrov, O. A.; Izmaylov, A. F.; Scuseria, G. E. Influence of the Exchange Screening Parameter on the Performance of Screened Hybrid Functionals. *J. Chem. Phys.* **2006**, *125* (22), 224106.
(44) Lu, T.; Chen, F. Multiwfn: A Multifunctional Wavefunction Analyzer. *J. Comput. Chem.* **2012**, *33* (5), 580−592.
(45) Mooibroek, T. J.; Gamez, P.; Reedijk, J. Lone Pair-π Interactions: A New Supramolecular Bond? *CrystEngComm* **2008**, *10* (11), 1501−1515.
(46) Lee, N.-S.; Shin, H.-K.; Kim, Y. J.; Kim, C.-H.; Suh, S.-H. HOMO-LUMO Energy Gap Analysis of Alkyl Viologen with a Positively Charged Aromatic Ring. *Rev. Roum. Chim.* **2010**, *55* (10), 627−632.
(47) Denning, R. G. Electronic Structure and Bonding in Actinyl Ions and Their Analogs. *J. Phys. Chem. A* **2007**, *111* (20), 4125−4143.
(48) Oher, H.; Réal, F.; Vercouter, T.; Vallet, V. Investigation of the Luminescence of $[UO_2X_4]^{2-}$ (X = Cl, Br) Complexes in the Organic Phase Using Time-Resolved Laser-Induced Fluorescence Spectroscopy and Quantum Chemical Simulations. *Inorg. Chem.* **2020**, *59* (9), 5896−5906.
(49) Oher, H.; Gomes, A. S. P.; Wilson, R. E.; Schnaars, D. D.; Vallet, V. How Does Bending the Uranyl Unit Influence Its Spectroscopy and Luminescence? *Inorg. Chem.* **2023**, *62* (24), 9273−9284.
(50) Matheson, M. S.; Lee, P. C.; Meisel, D.; Pelizzetti, E. Kinetics of Hydrogen Production from Methyl Viologen Radicals on Colloidal Platinum. *J. Phys. Chem.* **1983**, *87* (3), 394−399.
(51) Tsukahara, K.; Wilkins, R. G. Kinetics of Reduction of Eight Viologens by Dithionite Ion. *J. Am. Chem. Soc.* **1985**, *107* (9), 2632−2635.
(52) Ryan, M. D.; Wilson, G. S. Spectroelectrochemical evaluation of homogeneous electron transfer involving biological molecules. *Anal. Chem.* **1975**, *47* (6), 885−890.
(53) Guo, P. Y.; Sun, C.; Zhang, N. N.; Cai, L. Z.; Wang, M. S.; Guo, G. C. An Inorganic-Organic Hybrid Photochromic Material with Fast Response to Hard and Soft X-Rays at Room Temperature. *Chem. Commun.* **2018**, *54* (36), 4525−4528.
(54) Tao, C.; Wu, J.; Yan, Y.; Shi, C.; Li, J. A New Methylviologen-Templated Zinc Gallophosphate Zeolite with Photo-/Thermochromism, Fluorescent and Photoelectric Properties. *Inorg. Chem. Front.* **2016**, *3* (4), 541−546.
(55) Xu, G.; Guo, G.-C.; Wang, M.-S.; Zhang, Z.-J.; Chen, W.-T.; Huang, J.-S. Photochromism of a Methyl Viologen Bismuth(III) Chloride: Structural Variation Before and After UV Irradiation. *Angew. Chem.* **2007**, *119* (18), 3313−3315.
(56) Kruse, S.; Rajapaksha, H.; MacGillivray, L. R.; LaVerne, J. A.; Forbes, T. Atomistic level Effects of Noncovalent Interactions and Crystalline Packing for Organic Material Structural Integrity upon Exposure to Gamma Radiation. *Chem.—Eur. J.* **2023**, *29*, No. e202302653.
(57) Cowie, B. E.; Purkis, J. M.; Austin, J.; Love, J. B.; Arnold, P. L. Thermal and Photochemical Reduction and Functionalization Chemistry of the Uranyl Dication, [UVIO2]2+. *Chem. Rev.* **2019**, *119* (18), 10595−10637.
(58) Allen, D. M.; Burrows, H. D.; Cox, A.; Hill, R. J.; Kemp, T. J.; Stone, T. J. Absorption Spectrum and Reaction Kinetics of the Photoreactive State of the Uranyl Ion. *J. Chem. Soc., Chem. Commun.* **1973**, *2*, 59−60.
(59) Hill, R. J.; Kemp, T. J.; Allen, D. M.; Cox, A. Absorption Spectrum, Lifetime and Photoreactivity towards Alcohols of the

Excited State of the Aqueous Uranyl Ion (UO_2^{2+}). *J. Chem. Soc., Faraday Trans. 1* **1974**, *70*, 847−857.
(60) Volman, D. H.; Seed, J. R. The Photochemistry of Uranyl Oxalate. *J. Am. Chem. Soc.* **1964**, *86* (23), 5095−5098.
(61) Lu, G.; Haes, A. J.; Forbes, T. Z. Detection and Identification of Solids, Surfaces, and Solutions of Uranium Using Vibrational Spectroscopy. *Coord. Chem. Rev.* **2018**, *374*, 314−344.
(62) Carter, K. P.; Kalaj, M.; Kerridge, A.; Cahill, C. L. Probing Hydrogen and Halogen-Oxo Interactions in Uranyl Coordination Polymers: A Combined Crystallographic and Computational Study. *CrystEngComm* **2018**, *20* (34), 4916−4925.
(63) De Groot, J.; Cassell, B.; Basile, M.; Fetrow, T.; Forbes, T. Z. Charge-Assisted Hydrogen-Bonding and Crystallization Effects within UVI Glycine Compounds. *Eur. J. Inorg. Chem.* **2017**, *2017* (13), 1938−1946.
(64) Poizat, O.; Sourisseau, C.; Mathey, Y. Vibrational Study of the Methyl Viologen Dication MV^{2+} and Radical Cation MV^{o+} in Several Salts and as an Intercalate in Some Layered MPS_3 Compounds. *J. Chem. Soc., Faraday Trans. 1* **1984**, *80*, 3257−3274.
(65) Melendres, C. A.; Lee, P. C.; Meisel, D. Cyclic Voltammetry and In Situ Laser Raman Spectroscopy Studies of Electrogenerated Methyl Viologen Radical Cation. *J. Electrochem. Soc.* **1983**, *130* (7), 1523−1527.
(66) Lee, P. C.; Schmidt, K.; Gordon, S.; Meisel, D. Resonance Raman of Viologen Radicals. *Chem. Phys. Lett.* **1981**, *80* (2), 242−247.
(67) Tang, X.; Schneider, T. W.; Walker, J. W.; Buttry, D. A. Dimerized π-Complexes in Self-Assembled Monolayers Containing Viologens: An Origin of Unusual Wave Shapes in the Voltammetry of Monolayers. *Langmuir* **1996**, *12* (24), 5921−5933.
(68) Kumar, R.; Pillai, R. G.; Pekas, N.; Wu, Y.; McCreery, R. L. Spatially Resolved Raman Spectroelectrochemistry of Solid-State Polythiophene/Viologen Memory Devices. *J. Am. Chem. Soc.* **2012**, *134* (36), 14869−14876.
(69) Mishra, S.; Pandey, H.; Yogi, P.; Saxena, S. K.; Roy, S.; Sagdeo, P. R.; Kumar, R. Live Spectroscopy to Observe Electrochromism in Viologen Based Solid State Device. *Solid State Commun.* **2017**, *261*, 17−20.
(70) Redmond, M. P.; Cornet, S. M.; Woodall, S. D.; Whittaker, D.; Collison, D.; Helliwell, M.; Natrajan, L. S. Probing the Local Coordination Environment and Nuclearity of Uranyl(vi) Complexes in Non-Aqueous Media by Emission Spectroscopy. *Dalton Trans.* **2011**, *40* (15), 3914−3926.
(71) Yokoyama, Y.; Moriyasu, M.; Ikeda, S. Electron Transfer Mechanism in Quenching of Uranyl Luminescence by Halide Ions. *J. Inorg. Nucl. Chem.* **1976**, *38* (7), 1329−1333.
(72) Rehm, D.; Weller, A. Kinetics of Fluorescence Quenching by Electron and H-Atom Transfer. *Isr. J. Chem.* **1970**, *8* (2), 259−271.
(73) Cramer, S. D.; Covino, B. S. *Corrosion: Materials*; *Electrochemical Series*; ASM International, 2005.